

Nonlinear regimes of coherent optical phonon generation in quantum wells under electric current pumping

S. M. Komirenko and K. W. Kim

Department of Electrical and Computer Engineering, North Carolina State University, Raleigh, North Carolina 27695-7911, USA

V. A. Kochelap and V. V. Koroteev

Institute of Semiconductor Physics, National Academy of Sciences of Ukraine, Kiev-28, 252650, Ukraine

M. A. Stroschio

Department of Bioengineering and Electrical and Computer Engineering, University of Illinois at Chicago, Chicago, Illinois 60707, USA

(Received 28 February 2002; revised manuscript received 27 May 2003; published 14 October 2003)

We present an analysis of nonlinear regimes of the coherent optical phonon generation under the electron drift in quantum wells. The phonon and electron subsystems are treated self-consistently. This allows us to find the steady-state generation regimes with macroscopic populations of optical phonon modes and the electron transport controlled in part by the generated phonons. The generation regimes demonstrate a pronounced threshold character. At high electric fields above the threshold, practically single-mode generation occurs and the current-voltage characteristic is considerably changed. We demonstrate high efficiency generation of the coherent optical phonons by the electric current. The coherent macroscopic optical displacements and the amplitudes of oscillating electrostatic fields are evaluated. The proposed model based on the electron nonlinearities predicts a range of the pumping electric fields under which the steady state phonon generation is realized. Our results suggest that the phonon avalanche occurs beyond this field range.

DOI: 10.1103/PhysRevB.68.155308

PACS number(s): 73.23.-b, 72.20.Ht, 72.20.Dp, 85.35.Be

I. INTRODUCTION

Recent progress in the methods of excitation and detection of coherent high-frequency lattice vibrations (see Refs. 1 and 2 for a recent review) sparks an interest in the physics of coherent phonons and different applications of coherent phonon waves. High-frequency coherent acoustic and optical phonons have been observed for a number of semiconductor materials and heterostructures. These studies provide information on the excitation mechanisms, coherent phonon dynamics, electron-phonon interactions, and other important phenomena including the effects of interference of coherent lattice vibrations, phonon control of ionic motion,³ etc. Potential applications of coherent phonons include the utilization of phonons to improve the general performance of optoelectronic and microelectronic devices, as well as particular applications such as terahertz modulation of light,⁴ generation of high-frequency electric oscillations, manipulation with x rays,⁵ etc. Usually, high-frequency coherent phonons are excited optically by ultrafast laser pulses.^{1,2} For both fundamental phonon physics and practical applications, it is of importance to develop electrical methods of coherent phonon generation in semiconductor materials and heterostructures.

Amplification and generation of optical phonons by drifting electrons via the Cherenkov effect were proposed in the 1960's,⁶⁻⁸ but they were never realized for bulklike materials. This is because the Cherenkov amplification effect is possible only under the following stringent requirements: high electron drift velocities, large electron densities, and strong electron-optical phonon coupling. In bulk materials, it is practically impossible to meet these requirements and to compete with the high rate of phonon loss. However, the

outlook can be substantially different in short-channel or low-dimensional transport.

Very recently, direct observation of the optical phonon instability due to the electron drift was reported.⁹ The experiments were performed in short GaAs and InAs *p-i-n* structures. Ultrahigh drift velocities ($\approx 6 \times 10^7$ cm/s) and high electron concentrations ($> 10^{17}$ cm⁻³) were achieved under the transient velocity-overshoot transport.

The situation is more favorable in two-dimensional, confined structures. For example, it is well known that the modulation doped heterostructures can achieve the first two conditions (i.e., high electron drift velocities and large electron densities). Moreover, simultaneous confinement of electrons and optical phonons within the same quantum well (QW) provides the necessary strong coupling. Incidentally, our recent theoretical analysis¹⁰ illustrated that the Cherenkov effect can provide a large increment of *confined* optical phonon modes in high-quality modulation doped QW heterostructures with drift velocities¹¹ exceeding 1.5×10^7 cm/s for GaAs/AlAs and 2×10^7 cm/s for InAs/AlGaSb QW's. The increment is controlled by the electron drift velocity and, thus, by the applied electric field. As soon as the increment becomes larger than the inverse phonon lifetime for some phonon modes, the populations of these modes increase exponentially in time and the phonon subsystem becomes unstable. The instability is of a threshold effect and occurs for the electric fields above a critical magnitude.

The principal criterion of the Cherenkov effect is $V_{\text{dr}} > \omega_{\text{LO}}/q$ where V_{dr} is the electron drift velocity and ω_{LO} and q are the longitudinal optical (LO) phonon frequency and wave vector, respectively. This criterion reflects the formation of a population inversion of electron states resonantly interacting with the phonons (see, for example, Ref. 10).

Thus, a positive phonon increment corresponds to *stimulated emission* of the optical phonons. This allows one to suppose that the phonon instability could follow a scenario similar to that for lasers. Indeed, the population of the modes with a larger increment grows faster, resulting in the progressive narrowing of the phonon distribution function. However, the whole process cannot continue indefinitely and must be stabilized by some nonlinear mechanisms triggered by the presence of high phonon populations.

Motivated by the experimental observation of the LO-phonon instability,⁹ this paper investigates the *nonlinear* regimes of confined optical phonon generation in QW heterostructures under electric current pumping. By expanding the earlier work whose analysis was primarily limited to the linear, nondegenerate regime,¹⁰ the focus of the present work is to consider the influence of nonlinear processes, specifically the changes in the electron kinetics caused by the highly-nonequilibrium optical phonons themselves under the realistic degenerate conditions. Stimulated optical phonon emission proportional to the phonon population affects both the electron drift velocity and the electron temperature. In particular, an additional dissipation of the electron momentum and energy induced by the nonequilibrium phonons suppresses both the drift velocity and the electron temperature. These changes lead to a *reduction* in the increment. As soon as the maximum value of the increment approaches the inverse phonon lifetime, a competition between the growing modes occurs and the steady state regime is reached with generation of only a few phonon modes. It is demonstrated that the electron parameters such as the drift velocity, average energy, etc., change appreciably in the generation regime.

The rest of this paper is organized as follows. In Sec. II, we introduce the main definitions and formulate the basic equations. In Secs. III and IV, the nonlinear regimes are analyzed and discussed. The main conclusions are summarized in Sec. V.

II. BASIC EQUATIONS

The confined LO phonons in a QW can be characterized by two-dimensional phonon wave vectors \vec{q} and discrete (transverse) numbers m . For the population of the $\{\vec{q}, m\}$ mode, we introduce the kinetic equation

$$\frac{dN_{\vec{q},m}^-}{dt} = \gamma_{\vec{q},m}^{(+)}(1 + N_{\vec{q},m}^-) - \gamma_{\vec{q},m}^{(-)}N_{\vec{q},m}^- - \beta_{\vec{q},m}^-N_{\vec{q},m}^-, \quad (1)$$

where $N_{\vec{q},m}^-$ is the phonon population calculated per unit area of the QW layer and $\gamma_{\vec{q},m}^{(\pm)}$ are the parameters which determine the evolution of $N_{\vec{q},m}^-$ in time due to the interaction with two-dimensional electrons; $\gamma_{\vec{q},m}^{(\pm)}$ are strongly dependent on the electron distribution function. The parameter $\beta_{\vec{q},m}^-$ describes the phonon loss, which includes phonon scattering or phonon absorption due to nonelectronic mechanisms, phonon decay due to the lattice anharmonicity, etc. Equation (1) contains the terms corresponding to spontaneous and stimulated

processes. The latter terms can be represented as $\gamma_{\vec{q},m}^-N_{\vec{q},m}^- = (\gamma_{\vec{q},m}^{(+)} - \gamma_{\vec{q},m}^{(-)})N_{\vec{q},m}^-$ with the phonon increment (decrement)¹⁰

$$\gamma_{\vec{q},m}^- = \frac{4\alpha\omega_{\text{LO}}\sqrt{\Theta}G_m^2}{|\kappa_{el}|^2} \frac{\mathcal{J}^{(+)}(\Theta, \mathcal{V}, Q) - \mathcal{J}^{(-)}(\Theta, \mathcal{V}, Q)}{\mathcal{L}Q \left[Q^2 + \left(\frac{\pi m}{\mathcal{L}} \right)^2 \right]}. \quad (2)$$

Here, we introduce the Fröhlich electron-phonon coupling constant

$$\alpha = \frac{e^2}{\hbar} \sqrt{\frac{m^*}{2\hbar\omega_{\text{LO}}}} \left(\frac{1}{\kappa_{\infty}} - \frac{1}{\kappa_0} \right),$$

where κ_0 and κ_{∞} are the low-frequency and the high-frequency dielectric permittivities, respectively, e is the elementary charge, m^* is the effective mass of the electrons, κ_{el} is the electron permittivity calculated at the optical phonon frequency, n is the electron concentration, and $G_m = (-1)^m 8 / [\pi m(m^2 - 4)]$ with $m = 1, 3, 5, \dots$ (for the QW with infinitely high barriers).

The electron population factors \mathcal{J}^{\pm} are determined by the electron distribution. Following Ref. 10, we suppose that only the lower subband is populated by the two-dimensional electrons. Under the actual conditions of high electron concentrations, when the electron-electron scattering dominates over other collision mechanisms, this distribution can be thought of in the form of the shifted Maxwellian or Fermi-Dirac functions. In Ref. 10, the factors $\mathcal{J}^{(\pm)}(q)$ have been calculated for the nondegenerate electrons with the use of a shifted Maxwellian function. In this paper, we generalize these calculations assuming the electron distribution in the form of a shifted Fermi-Dirac function \mathcal{F} with two parameters, the electron temperature T_e and the drift velocity V_{dr} :

$$\mathcal{F}(V) = \left(1 + \exp \left[\frac{m^*(\mathbf{V} - \mathbf{V}_{\text{dr}})^2}{2k_B T_e} - \frac{E_F}{k_B T_e} \right] \right)^{-1},$$

where the quasi-Fermi level E_F is found from the normalization condition at a given electron concentration n . Thus E_F depends on n , T_e , and V_{dr} . Now for the factors $\mathcal{J}^{(\pm)}(q)$ we obtain

$$\mathcal{J}^{(\pm)}(\Theta, \mathcal{V}, Q) = \int_0^{\infty} \frac{dy}{\sqrt{y} [1 + D^{(\pm)} \exp(y)]}, \quad (3)$$

$$D^{(\pm)} = \exp \left[\frac{1}{4\Theta} \left(\frac{1}{Q} \pm Q - 2\mathcal{V} \right)^2 - \frac{\zeta_F + \mathcal{V}^2}{\Theta} \right].$$

In Eqs. (2) and (3), we introduce the dimensionless parameters

$$\Theta = \frac{k_B T_e}{\hbar \omega}, \quad \mathcal{V} = \frac{V_{\text{dr}}}{V_O}, \quad Q = \frac{q}{k_O},$$

$$\mathcal{L} = L k_O, \quad \zeta_F = \frac{E_F - m^* V_{\text{dr}}^2 / 2}{\hbar \omega}$$

with the QW width L . Throughout the paper, we use the characteristic velocity, momentum, and electric field

$$V_o = \sqrt{\frac{2\hbar\omega_{LO}}{m^*}}, \quad k_o = \frac{\sqrt{2m^*\hbar\omega_{LO}}}{\hbar}, \quad F_o = \frac{4\pi\alpha\hbar\omega_{LO}}{eL}.$$

It is worth noting that γ_q of Eq. (2) is defined for the wave vector directed along the electron drift. For the general case of $\mathbf{q} = \{q_x, q_y\}$, the γ_q dependence can be obtained from Eq. (2) by the substitution $V_{dr} \rightarrow V_{dr} \times \sqrt{q^2 - q_y^2}/q$.

The parameters T_e and V_{dr} should be found from the energy and momentum balance equations

$$\frac{d\langle E \rangle}{dt} = eFV_{dr} - Q_E(T_e, V_{dr}), \quad (4)$$

$$\frac{d\langle m^*V \rangle}{dt} = eF - Q_M(T_e, V_{dr}). \quad (5)$$

Here $Q_E(T_e, V_{dr})$ and $Q_M(T_e, V_{dr})$ designate the dissipation rates of average electron energy $\langle E \rangle$ and momentum $\langle m^*V \rangle$ per electron, respectively. For the steady state case, the time derivatives equal zero.

Optical phonon generation can be achieved when a high electric field is applied. Under this condition, scattering by the confined optical phonons is typically the dominant mechanism for the energy and momentum dissipation of the two-dimensional electrons. Now the dissipation rates in Eqs. (4) and (5) can be presented as

$$Q_E = Q_E^{eq}(T_e, V_{dr}) + \sum_{q,m} \hbar\omega_{LO} \gamma_{q,m}^- \frac{N_{q,m} - N_{eq}}{n}, \quad (6)$$

$$Q_M = Q_M^{eq}(T_e, V_{dr}) + \sum_{q,m} \hbar q \gamma_{q,m}^- \frac{N_{q,m} - N_{eq}}{n}. \quad (7)$$

The first terms represent the dissipation through equilibrium optical phonons and the second terms are the contributions of excess (generated) phonons to the dissipation; N_{eq} is the Planck function with the lattice temperature T_l . Q_E^{eq} and Q_M^{eq} can be expressed via the dimensionless functions $\mathcal{E}^{eq}(\Theta, \mathcal{V})$ and $\mathcal{M}^{eq}(\Theta, \mathcal{V})$:

$$Q_E^{eq} = \frac{eF_o V_o k_o^2}{4\pi^2 n} \mathcal{E}^{eq}, \quad Q_M^{eq} = \frac{eF_o k_o^2}{4\pi^2 n} \mathcal{M}^{eq}. \quad (8)$$

Particular expressions for these functions will be provided elsewhere.

In a generation regime, the population of some modes considerably exceeds the equilibrium value N . The steady state population can be found from Eq. (1):

$$N_{q,m}^- = \frac{\gamma_{q,m}^{(+)}}{\beta_{q,m}^- - \gamma_{q,m}^-}. \quad (9)$$

Equations (2)–(9) compose the system, which self-consistently determines the phonon population $N_{q,m}^-$, the drift velocity V_{dr} , and the electron temperature T_e at a given electric field F under the steady state.

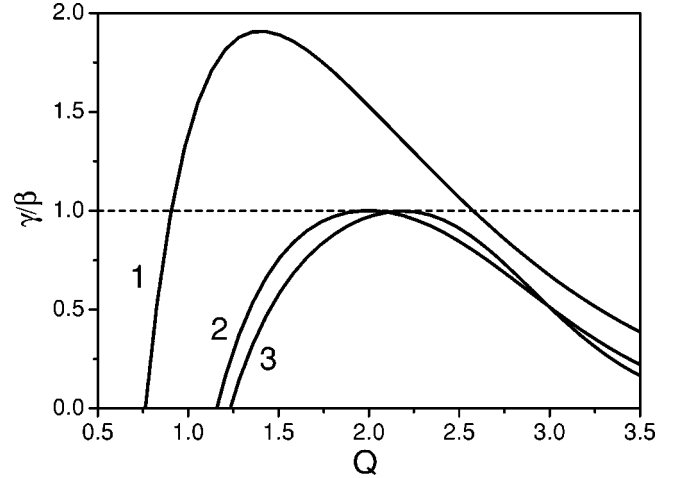


FIG. 1. Increment γ versus wavevector Q as a function of dimensionless electric field f in a 100 Å GaAs QW with $\beta = 2.7 \times 10^{11} \text{ s}^{-1}$. Curves 1 and 2 show the results of the linear and nonlinear analyses, respectively, at $f = 0.09$ that is above the threshold field. Curve 3 is at the threshold of generation $f = 0.047$.

III. ANALYSIS OF NONLINEAR REGIMES

We start with a brief discussion of the effect of the Fermi-Dirac statistics on the sign and the magnitude of the decrement γ_q . From Eqs. (2) and (3), one can see that the sign of γ_q is determined by

$$\text{sgn}[e^{(1/Q+Q-2)^2} - e^{(1/Q-Q-2)^2}]$$

and does not depend on the electron degeneracy level. Then we find that at $n > 10^{12} \text{ cm}^{-2}$ and $V_{dr} > 1.7 \times 10^7 \text{ cm/s}$, the magnitude of γ_q exceeds 10^{11} s^{-1} as in the case of the non-degenerate electrons.¹⁰ In the absence of the generation (i.e., linear analysis), the typical $\gamma(Q)$ dependence is as illustrated in Fig. 1 by curve 1. Note that the screening due to the degenerate electrons is small at the optical phonon frequency; its contribution to γ is estimated to be approximately 2–5 %.

For further nonlinear analysis, two conclusions made in the linear theory of phonon instability¹⁰ are important: (i) the phonon increment $\gamma_{q,m}^-$ has a maximum γ_M at a certain wave vector q_M and (ii) only the modes with the lowest transverse index $m = 1$ (i.e., the largest γ_M) can be generated (below we will drop this index). Likewise, the contribution of other types of QW phonon modes such as the interface phonons can be ignored in relatively wide QW's as they are dominated by the confined modes. This should result in a strong selection of generated modes, as it holds in lasers,¹² with nearly identical wavevectors. Now we can use the so-called single-mode approximation well known from laser physics. Under this approximation, we can introduce the total number of highly coherent generated phonons $N_{\text{cph}} = \sum_q N_q^- (\gg N)$ and adopt the steady-state condition of generation, namely, the gain-loss balance $\gamma_M = \beta$. Finally, for the dimensionless electron temperature Θ , drift velocity \mathcal{V} , and the density of the generated phonons

$$\mathcal{N} = \frac{N_{\text{cph}}}{N_O}, \quad N_O \equiv \frac{eF_O V_O}{\hbar \omega_{\text{LO}} \beta} n, \quad (10)$$

we obtain the following nonlinear *algebraic* equations:

$$\beta = \gamma_M[\Theta, \mathcal{V}], \quad (11)$$

$$f\mathcal{V} = \mathcal{E}_{\text{eq}}[\Theta, \mathcal{V}] + \mathcal{N}, \quad (12)$$

$$f = \mathcal{M}_{\text{eq}}[\Theta, \mathcal{V}] + Q_M \mathcal{N}. \quad (13)$$

Here $f = F/F_O$ is the dimensionless field. In general, γ_M depends on \mathcal{N} via Θ and \mathcal{V} , and has to be calculated at $Q = q_M/k_O$. The latter should be found from the additional equation

$$d\gamma/dQ = 0. \quad (14)$$

These equations contain the three ‘‘controlling’’ parameters—electric field f , the phonon loss β , and the QW width \mathcal{L} . The advantage of the derived system of equations is that the dimensionless solutions can be used to evaluate the generation regimes for the three given parameters in any semiconductor materials to which the model of confined polar optical phonons is applicable.

Having found the number of generated phonons N_{cph} in the single-mode approximation, one can estimate the range of generated phonon wave vectors $\Delta \mathbf{q}$. For this we should account for the phonons with nonzero wavevector projection q_y , which can also be generated. From Eq. (9) we have $N_{\text{cph}} = \sum_{\mathbf{q}} \gamma_{\mathbf{q}}^{(+)} / (\beta - \gamma_{\mathbf{q}})$, where $\mathbf{q} = \{q_x, q_y\}$. Using the expansion in series $\gamma_{\mathbf{q}} = \gamma_M - [\gamma_{q_x}''(q_x - q_M)^2 + \gamma_{q_y}''q_y^2]/2$, we find the following estimation for Δq_x :

$$\Delta q_x \approx \sqrt{\frac{\gamma_M}{\gamma_{q_x}''}} \exp \left[-\frac{\pi N_{\text{cph}} \sqrt{\gamma_{q_x}'' \gamma_{q_y}''}}{\gamma_M} \right]. \quad (15)$$

The expression for Δq_y can be obtained from Eq. (15) by the substitution $\gamma_{q_x}'' \rightarrow \gamma_{q_y}'' = V_{\text{dr}}(\partial \gamma_M / \partial V_{\text{dr}}) / q_M^2$ in the preexponential factor. One can see that the range of generated phonon wave vectors narrows exponentially as the phonon population increases.

Prior to presenting the numerical results, some general conclusions can be drawn from the qualitative comparison of the electron parameters in the absence of generation (i.e., linear analysis) and those under a generation regime. In the former case, as it follows from Eqs. (4), (5), and (8), the drift velocity \mathcal{V} and the electron temperature Θ are related via the expression independent of the field: $\mathcal{V} = \mathcal{E}_{\text{eq}}(\Theta, \mathcal{V}) / \mathcal{M}(\Theta, \mathcal{V})$. It gives us a dependence $\mathcal{V}_{\text{kin}}(\Theta)$ determined by the total rates of energy and momentum dissipation. In Fig. 2(a), we present this $\mathcal{V}_{\text{kin}}(\Theta)$ dependence by curve 1. In the generation regime, \mathcal{V} and Θ are related via Eq. (11), which is determined by the gain-loss balance of the coherent phonons. The corresponding $\mathcal{V}_{\text{gen}}(\Theta)$ dependences are curves 2, 3, and 4 in Fig. 2(a) for different β . Excluding f from Eqs. (12) and (13), we obtain $\mathcal{N} = [\mathcal{E}_{\text{eq}} - \mathcal{V} \mathcal{M}_{\text{eq}}] / [2Q_M \mathcal{V} - 1]$. It is easy to check that the denominator in this formula is positive when

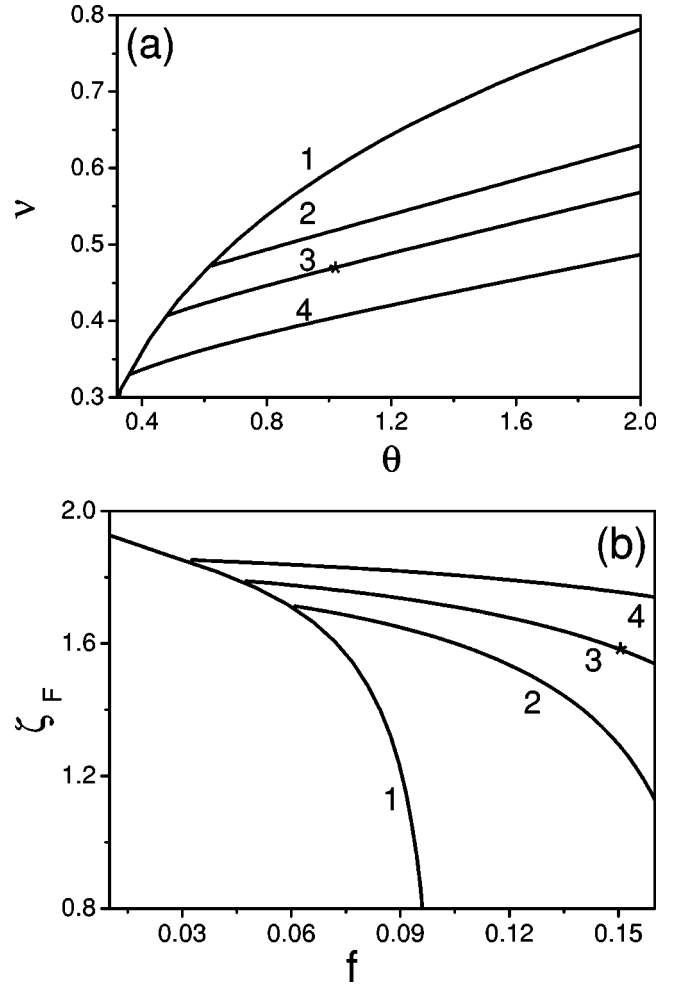


FIG. 2. (a) Dimensionless drift velocity $\nu(\Theta)$ and (b) quasi-Fermi level $\zeta_F(f)$. Curve 1 represents the linear analysis, while curves 2, 3, and 4 correspond to the results of nonlinear analyses with $\beta = 3.4 \times 10^{11} \text{ s}^{-1}$, $2.7 \times 10^{11} \text{ s}^{-1}$, and $1.9 \times 10^{11} \text{ s}^{-1}$, respectively. The star denotes the result for $f = 0.15$ ($F = 4.7 \text{ kV/cm}$) and $\beta = 2.7 \times 10^{11} \text{ s}^{-1}$.

the Cherenkov condition is met. Thus, for the generation regime ($\mathcal{N} > 0$), we find the inequality $\mathcal{E}(\Theta, \mathcal{V}) - \mathcal{V} \mathcal{M}(\Theta, \mathcal{V}) > 0$. The latter means that the electron parameters under the generation fall into the part of the $\mathcal{V}-\Theta$ plane restricted from the above by the curve $\mathcal{V}_{\text{kin}}(\Theta)$. The crossings of the curves $\mathcal{V}_{\text{gen}}(\Theta)$ and $\mathcal{V}_{\text{kin}}(\Theta)$ determine the critical (threshold) points of generation regimes.

We solved Eq. (12) for different parameters. In Figs. 1–5, we show the results obtained for the 100 Å GaAs QW with three values of phonon loss β . From these figures, the following conclusions can be made concerning the general behavior of the electron-phonon system under the generation regime. The phonon density-electric field dependence demonstrates a pronounced threshold character: $\mathcal{N} = 0$ at $f < f_{\text{th}}$, while \mathcal{N} rapidly increases for $f > f_{\text{th}}$. The threshold field satisfies the condition $\gamma_M(f_{\text{th}}) = \beta$ at $\mathcal{N} = 0$. Accordingly, the larger the phonon loss is, the higher the threshold field becomes. Below the threshold, the maximum of the phonon increment increases with the field. Once the thresh-

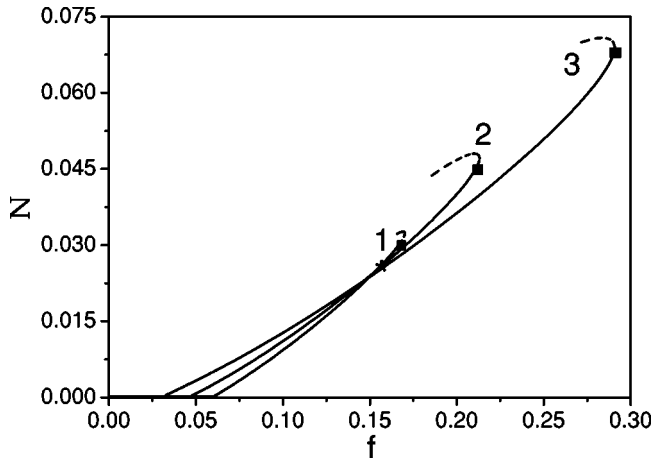


FIG. 3. Nonequilibrium phonon population versus applied field. Curves 1, 2, and 3 are for $\beta=1.9 \times 10^{11} \text{ s}^{-1}$, $2.7 \times 10^{11} \text{ s}^{-1}$, and $3.4 \times 10^{11} \text{ s}^{-1}$, respectively. The critical points $[\mathcal{N}_{cr}, f_{cr}]$ are indicated by the black squares. The unstable branches are shown by the dashed lines. As in Fig. 2, the star denotes the result for $f=0.15$ ($F=4.7 \text{ kV/cm}$) and $\beta=2.7 \times 10^{11} \text{ s}^{-1}$.

old is reached, further increase in the increment is suppressed and its maximum (which equals exactly to the phonon loss β) occurs at a smaller Q as illustrated in Fig. 1. In this figure, curves 3 and 2 are obtained for the threshold field and a field of the developed generation, respectively, while the phonon loss is kept the same. For comparison, we also provide the increment (curve 1) calculated without taking the nonlinear process into account as for curve 1 of Fig. 2. In laser physics, the light gain is analogous to the phonon increment studied in this paper. The behavior predicted for the increment is typical for the gain under laser generation.

In Fig. 3, we present the results obtained for the generated

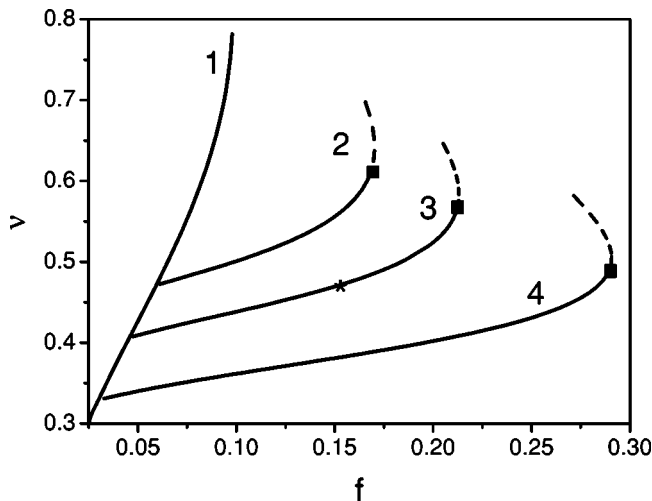


FIG. 4. Electron drift velocity versus applied field. Curve 1 represents the linear analysis while curves 2, 3, and 4 correspond to the results of nonlinear analyses with $\beta=3.4 \times 10^{11} \text{ s}^{-1}$, $2.7 \times 10^{11} \text{ s}^{-1}$, and $1.9 \times 10^{11} \text{ s}^{-1}$, respectively. The critical points $[\mathcal{N}_{cr}, f_{cr}]$ are indicated by the black squares. The unstable branches are shown by the dashed lines. As in Fig. 2, the star denotes the result for $f=0.15$ ($F=4.7 \text{ kV/cm}$) and $\beta=2.7 \times 10^{11} \text{ s}^{-1}$.

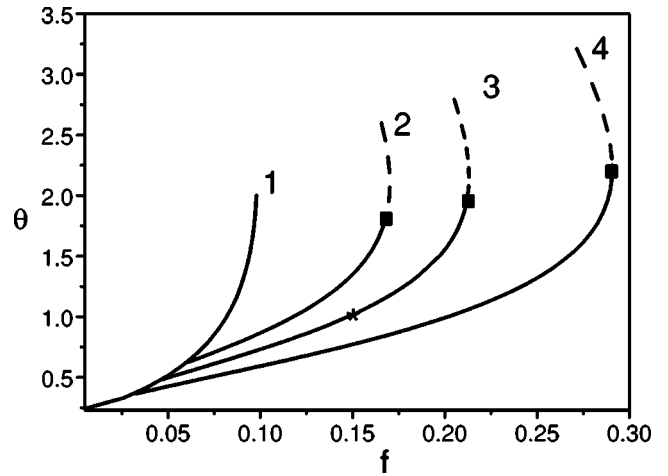


FIG. 5. Electron temperature versus applied field. Curve 1 represents the linear analysis while curves 2, 3, and 4 correspond to the results of nonlinear analyses with $\beta=3.4 \times 10^{11} \text{ s}^{-1}$, $2.7 \times 10^{11} \text{ s}^{-1}$, and $1.9 \times 10^{11} \text{ s}^{-1}$, respectively. The critical points $[\mathcal{N}_{cr}, f_{cr}]$ are indicated by the black squares. The unstable branches are shown by the dashed lines. As in Fig. 2, the star denotes the result for $f=0.15$ ($F=4.7 \text{ kV/cm}$) and $\beta=2.7 \times 10^{11} \text{ s}^{-1}$.

phonon density \mathcal{N} with different phonon losses. The $\mathcal{N}(f)$ dependence calculated for a given phonon loss β behaves almost linearly in a range of the electric field above the threshold. As the field increases, however, the $\mathcal{N}(f)$ curve turns up reaching a critical value \mathcal{N}_{cr} at a field $f_{cr}(\beta)$. No stationary solution exists at $f > f_{cr}$ for the proposed model. Instead, we obtain a second (upper) branch of the $\mathcal{N}(f)$ dependence at $f < f_{cr}$.

Typically such a “branching” may lead to unstable solutions. We can check the stability of these solutions as follows. Let \mathcal{N} , Θ , \mathcal{V} , and q_M be solutions of the nonlinear algebraic equations [Eqs. (11)–(14)] discussed previously. We introduce small time-dependent deviations for these variables $\delta\mathcal{N}$, $\delta\Theta$, $\delta\mathcal{V}$, and δq_M , which are governed by the linearized time-dependent differential equations [Eqs. (1), (4), and (5)] and the algebraic equation [Eq. (14)]. The solutions of these linear equations have the functional form

$$\delta\mathcal{N}, \delta\Theta, \delta\mathcal{V}, \delta q_M \propto e^{\lambda\tau} \tag{16}$$

with $\tau = \beta t$. The system of differential equations of the third order gives us three values for the decrement $\lambda_1, \lambda_2, \lambda_3$. If $\lambda_1, \lambda_2, \lambda_3 < 0$, the deviations decrease with time and the initial state characterized by parameters \mathcal{N} , Θ , \mathcal{V} , and q_M is stable. If at least one of $\lambda_1, \lambda_2, \lambda_3$ is positive, then the initial state is unstable. Applying this analysis, we found that the second branch is always kinetically unstable.

Interestingly, the abovementioned system of differential equations [Eqs. (1), (4), and (5)] is characterized by two different time scales: the momentum and energy relaxation is determined by the transport time τ_{tr} , while the time evolution of the phonons is of the order of the inverted increment $1/\gamma$. It is easy to see that $\tau_{tr}/\gamma \ll 1$. This implies that the absolute value of one of the lambdas ($\lambda_{1,2,3}$) which is associated with the phonon kinetic equation of Eq. (1), is always

smaller than the absolute values of the other two, say $|\lambda_1| \ll |\lambda_{2,3}|$. At $f=f_{\text{cr}}$, just this smallest λ_1 changes its sign. It means that the instability at $f \geq f_{\text{cr}}$ is led mainly by the phonon equation. This allows one to suggest that at $f \geq f_{\text{cr}}$ the optical phonon avalanche takes place.

The generation of optical phonons affects appreciably the electron parameters, as seen from Figs. 4 and 5. At a given field above the threshold, both the electron drift velocity (Fig. 4) and the electron temperature (Fig. 5) decrease while the quasi-Fermi level [Fig. 2(b)] increases, in comparison to the case when the generation is suppressed (i.e., curve 1). Apparently, these effects—deceleration and cooling of the electrons—are due to the energy and momentum transfer from the electrons to the generated phonons. At a given phonon loss, the stationary solutions for $\Theta(f)$ and $\mathcal{V}(f)$ exist in a finite range of the electric fields. There are also unstable branches, as presented in Figs. 4 and 5. In polar materials, high fields can induce the so-called electron runaway effect,¹³ namely, the rapid increase in the electron temperature and the drift velocity. In Figs. 4 and 5, the beginning of the runaway effect appears as a sharp “turn-up” in the high-field parts of $\Theta(f)$ and $\mathcal{V}(f)$ dependences. From our results, it follows that the runaway effect is canceled under the optical phonon generation regime. Instead, we obtain the optical phonon avalanche in the high field range at $f \geq f_{\text{cr}}$.

We conclude this brief analysis of the generation regime by mentioning that the developed model is based on the so-called electron nonlinearity, i.e., the changes in the electron characteristics Θ and \mathcal{V} due to the nonequilibrium optical phonon population. The model predicts a stable steady-state generation regime for a finite field range after the threshold. We found that the stability is broken at high phonon populations. Under this condition, phonon nonlinearities can also become of importance. These include the mechanisms that lead to an increase in the optical phonon loss. The examples are the self-stimulated optical phonon decay,¹⁴ the Joule heating resulting in an increase of β , etc. These mechanisms can stabilize the generation regime at high electric fields. They will be analyzed elsewhere.

IV. NUMERICAL ESTIMATES AND DISCUSSION

Now, we can apply the above results to specific heterostructures. First we consider a selectively *n*-doped AlAs/GaAs/AlAs QW. Taking $m^*=0.067m_0$, $\hbar\omega_{\text{LO}}=36.3$ meV (8.9 THz), $\kappa_0=12.4$ and $\kappa_\infty=10.6$, where m_0 is the free electron mass, we find the parameters $\alpha=0.069$, $k_O=2.53 \times 10^6$ cm⁻¹, $V_O=4.36 \times 10^7$ cm/s, and $F_O=31.3$ kV/cm (for the latter three parameters, a QW of 100 Å in width is considered). We assume the lattice temperature $T_l=100$ K. Then the phonon loss due to the lattice anharmonicity is $\beta=1.9 \times 10^{11}$ s⁻¹.¹⁵ For the electron concentration $n=2 \times 10^{12}$ cm⁻², we find the threshold field $f_{\text{th}}=0.033$ ($F_{\text{th}}=1$ kV/cm), corresponding velocity $\mathcal{V}_{\text{th}}=0.3$ ($V_{\text{dr}}=1.4 \times 10^7$ cm/s) and temperature $\Theta_{\text{th}}=0.39$ ($T_e=130$ K). The maximum γ occurs at $q_M/k_O=2.46$. The high-field boundary of the steady state regime is characterized by the following critical parameters $f_{\text{cr}}=0.29$ ($F_{\text{cr}}=9$ kV/cm), corresponding velocity $\mathcal{V}=0.5$ ($V_{\text{dr}}=2.2$

$\times 10^7$ cm/s), temperature $\Theta=0.39$ ($T_e=130$ K), $q_M/k_O=1.65$ and the phonon density $\mathcal{N}=0.069$ ($N_O=4 \times 10^{14}$ cm⁻², $N_{\text{cph}}=1.86 \times 10^{13}$ cm⁻²).

For the larger phonon losses used in Figs. 2–5, we obtain $f_{\text{th}}=0.047$ ($F=1.4$ kV/cm), $\mathcal{V}_{\text{th}}=0.4$ ($V_{\text{dr}}=1.7 \times 10^7$ cm/s), $\Theta_{\text{th}}=0.47$ ($T_e=200$ K) at $\beta=2.7 \times 10^{11}$ s⁻¹ and $f_{\text{th}}=0.06$ ($F=1.9$ kV/cm), $\mathcal{V}_{\text{th}}=0.47$ ($V_{\text{dr}}=2 \times 10^7$ cm/s), $\Theta_{\text{th}}=0.61$ ($T_e=260$ K) at $\beta=3.4 \times 10^{11}$ s⁻¹.

As an example of the developed generation regime, we first consider the moderate pumping field $f=0.15$ ($F=4.7$ kV/cm) supposing the phonon loss $\beta=2.7 \times 10^{11}$ s⁻¹, which is marked by the star in Figs. 2–5. We find the area phonon density $\mathcal{N}=0.024$ ($N_O=2.7 \times 10^{14}$ cm⁻², $N_{\text{cph}}=6.8 \times 10^{12}$ cm⁻²) and the electron parameters $\Theta=1.03$ ($T_e=430$ K), and $\mathcal{V}=0.47$ ($V_{\text{dr}}=2 \times 10^7$ cm/s). Parameters $\lambda_{1,2,3}$, which determine the stability of the solution according to Eq. (16), are -1 , -3.5 , and -36 . Then, the maximum of the phonon populations occurs at $q_M/k_O=1.8$. Equation (15) predicts a width of the generated wave vector range $\Delta q_x=4.7 \times 10^5$ cm⁻¹, $\Delta q_y=7 \times 10^5$ cm⁻¹. Setting the lateral dimensions of the QW layer $L_x=L_y=1$ μm, we obtain for this example that one longitudinal and two transverse optical phonon modes are generated. It is instructive to compare these figures with the number of the phonon modes effectively interacting with electrons. The latter number is estimated to be $q_M^2 L_x L_y / 4\pi \approx 2 \times 10^4$.

As another example, we consider the case of the maximal steady-state field f_{cr} at the same phonon loss. The parameters $\lambda_{1,2,3}$ are 0, -0.3 and -40 , which correspond to the threshold of instability. The phonon density is $\mathcal{N}=0.047$ ($N_{\text{cph}}=1.3 \times 10^{13}$ cm⁻¹). The maximum of the phonon population is at $q_M/k_O=1.5$. The generated wave vector range ($\Delta q_x=1.5 \times 10^2$ cm⁻¹, $\Delta q_y=2 \times 10^2$ cm⁻¹) is appreciably smaller than the intermode spacing ($\approx \pi/L_x, \pi/L_y$) in a realistic finite-size QW layer. Thus for this case, a one-mode (i.e., highly coherent) generation regime occurs (in the contrast to multimode generation near the threshold).

Now we analyze two other quantities characterizing the generated optical phonons that can be of interest. Consider, for example, the optical displacement of ions in the primitive cell. According to Ref. 10, the displacement vector of the confined LO phonons has two components—one is parallel to the wave vector $\mathbf{q}=\{q,0,0\}$ and the other perpendicular to the QW layer:

$$\mathbf{u}_{q,l} = \sqrt{\frac{\hbar\Omega_0 N_{\text{cph}}}{M\omega_{\text{LO}}L}} \frac{e^{i(q_x x + q_y y - \omega t)}}{\sqrt{q^2 + (\pi/L)^2}} \times \begin{cases} iq_l \cos\left[\frac{\pi z}{L}\right], & l=x, \\ -\frac{\pi}{L} \sin\left[\frac{\pi z}{L}\right], & l=z. \end{cases}$$

Here, Ω_0 is the volume of the primitive crystal cell and M is the reduced mass of the ions. For the developed generation regime, the magnitude of the *coherent* optical displacement in the middle of the QW layer is estimated to be 0.014% of the lattice constant of GaAs. Next, the alternative electric field conveying the optical vibrations is

$$\tilde{\mathbf{F}}(t) = -\frac{4\pi\omega_{LO}}{\kappa_\infty} \sqrt{\frac{\mathcal{M}}{4\pi\Omega_0} \left(\frac{1}{\kappa_\infty} - \frac{1}{\kappa_0} \right)} \mathbf{u}_q(t).$$

In the generation regime, the amplitude of this oscillating *macroscopic* field is of the order of 6 kV/cm.

Now, we shall briefly present the results for InAs QW layers. Bulk InAs exhibits electron drift velocity twice that of GaAs. Thus the strained InAs QW's sandwiched between the AlGaSb barriers can demonstrate a large Cherenkov effect for generation of coherent optical phonons.¹⁰ The following parameters can be taken to describe the 100 Å InAs QW: $\hbar\omega_{LO}=29.5$ meV (7 THz), $\alpha=0.059$, $k_O=1.55 \times 10^6$ cm⁻¹, $V_O=5.88 \times 10^7$ cm/s, $F_O=21.6$ kV/cm. By applying the developed theory to the InAs QW, we obtain the results very similar to those discussed above for the GaAs QW's. For example, with $n=10^{12}$ cm⁻² and $\beta=10^{11}$ s⁻¹, we find that the threshold of generation occurs at $f_{th}=0.02$ ($F=0.45$ kV/cm), $\mathcal{V}_{th}=0.31$ ($V_{dr}=1.8 \times 10^7$ cm/s), $\Theta=0.52$ ($T_e=180$ K), $q_M/k_O=2.83$. For the regime of developed generation at $f=0.06$ ($F=1.2$ kV/cm), we find $\mathcal{V}=0.35$ ($V_{dr}=2 \times 10^7$ cm/s) and $\Theta=0.84$ ($T_e=290$ K). The generated phonon density is $\mathcal{N}=0.006$ ($\mathcal{N}_O=3.6 \times 10^{14}$ cm⁻², $N_{cph}=2.1 \times 10^{12}$ cm⁻²). For $L_x=L_y=1$ μm, the number of generated longitudinal and transverse confined modes are 7 and 14, respectively.

The approach developed in this paper allows one to evaluate the efficiency of electric power transformation to the generated optical phonons. We can define this efficiency as the ratio of the power dissipated via the generated phonons to the total electric power dissipated in the crystal:

$$\eta = \frac{\beta \hbar \omega N_{cph}}{e F V n} = \frac{\mathcal{N}}{f v}.$$

The η - f dependence is presented in Fig. 6 for the example of GaAs/AlGaAs QW. It can be seen that the efficiency increases with f reaching the magnitudes well above 30% under the developed phonon generation.

V. CONCLUSION

We analyzed the generation of confined optical phonons in QW's under the electric pumping. To treat the phonon and drifting electron subsystems self-consistently, we calculated the phonon increment as a function of electron temperature and drift velocity, while in the balance equations of the electron energy and momentum we incorporated the terms describing the energy and momentum loss due to coherent phonon emission. Fermi-Dirac statistics are assumed to describe the electron distributions. By solving the coupled nonlinear equations, we found steady-state generation regimes with macroscopic populations of the optical phonon modes and

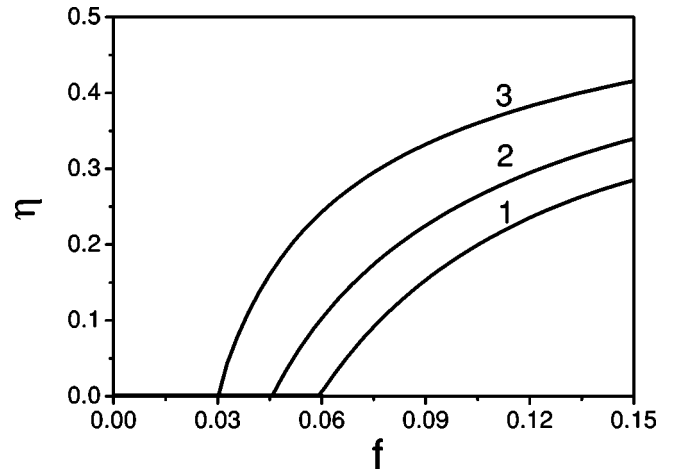


FIG. 6. Efficiency of the energy conversion under the phonon generation as a function of the field for different values of β . Curves 1, 2, and 3 correspond to $\beta=3.4 \times 10^{11}$ s⁻¹, 2.7×10^{11} s⁻¹, and 1.9×10^{11} s⁻¹, respectively.

electron transport that is controlled significantly by the generated phonons.

These generation regimes have a pronounced threshold character. Above the threshold electric field, fast narrowing of the range of the generated phonon wave vectors occurs. Under high fields, this practically results in a single-mode generation. The generated mode is highly populated, which leads to *coherent macroscopic* optical displacements of the lattice and large oscillation amplitudes of the electrostatic fields conveying the optical vibrations.

The proposed model based on the electron nonlinearities predicts a range of the pumping electric fields for steady-state phonon generation. We suggest that beyond this range, the phonon avalanche occurs and a new steady state can be achieved when phonon nonlinearities come into the play.

We established that the electron parameters, such as the temperature and drift velocity, are affected by the generated phonons; their magnitudes are suppressed considerably at a given electric field. Finally, we estimated the transformation efficiency of the electric power to coherent optical vibrations. This analysis confirms that pumping by the electric current can be an efficient method for coherent optical phonon generation in quantum heterostructures.

ACKNOWLEDGMENTS

This work was supported by the Air Force Office of Scientific Research through the MURI program, the U.S. Army Research Office, and the CRDF (Grant No. UV2-2439-KV-02).

¹W.A. Kutt, W. Albrecht, and H. Kurz, IEEE J. Quantum Electron. **QE-28**, 2434 (1992).

²R. Merlin, Solid State Commun. **102**, 207 (1997).

³X. Hu and F. Nori, Physica B **263-264**, 16 (1999).

⁴T.K. Chen, L.H. Acioli, J. Vidal, H.J. Zeiger, G. Dresselhaus, M.S. Dresselhaus, and E.P. Ippen, Appl. Phys. Lett. **62**, 1901 (1993).

⁵P.H. Bucksbaum and R. Merlin, Solid State Commun. **111**, 535

- (1999); D.A. Reis, M.F. DeCamp, P.H. Bucksbaum, R. Clarke, E. Dufresne, M. Hertlein, R. Merlin, R. Falcone, H. Kapteyn, M.M. Murnane, J. Larsson, Th. Missalla, and J.S. Wark, *Phys. Rev. Lett.* **86**, 3072 (2001).
- ⁶V.L. Gurevich, *Sov. Phys. Solid State* **4**, 1380 (1962).
- ⁷I.A. Chaban and A.A. Chaban, *Sov. Phys. Solid State* **6**, 2411 (1964).
- ⁸J.B. Gunn, *Phys. Rev.* **138**, A1721 (1965).
- ⁹W. Liang, K.T. Tsen, O.F. Sankey, S.M. Komirenko, K.W. Kim, V.A. Kochelap, M.C. Wu, C.L. Ho, W.J. Ho, and H. Morkoç, *Appl. Phys. Lett.* **82**, 1968 (2003).
- ¹⁰S.M. Komirenko, K.W. Kim, V.A. Kochelap, I. Fedorov, and M.A. Stroscio, *Appl. Phys. Lett.* **77**, 4178 (2000); *Phys. Rev. B* **63**, 165308 (2001).
- ¹¹For comparison, in bulk GaAs and GaAs/AlGaAs heterostructures peak drift velocities higher than 2×10^7 cm/s and 3.5×10^7 cm/s were measured at 300 and 77 K, respectively. See W.T. Masselink, *Semicond. Sci. Technol.* **4**, 503 (1989).
- ¹²R. Loudon, *The Quantum Theory of Light* (Clarendon, Oxford, 1973).
- ¹³E.M. Conwell, *High Field Transport in Semiconductors* (Academic, New York, 1967).
- ¹⁴D.A. Romanov, B.A. Glavin, V.V. Mitin, and M.A. Stroscio, *Phys. Rev. B* **60**, 4771 (1999).
- ¹⁵F. Vallee and F. Bogani, *Phys. Rev. B* **43**, 12049 (1991); F. Vallee, *ibid.* **49**, 2460 (1994).